Nonlinear Slosh Damping Testing and Analysis for Launch Vehicle Propellant Tanks

Tannen S. VanZwieten[1]
Langley Research Center, Hampton, Virginia, 23691, USA

Jacob M. Brodnick[2]
Jacobs Technology Inc., Huntsville, Alabama, 35806, USA

Shane Reese[3]
Brigham Young University, Provo, Utah, 84602, USA

Michael Ruth[4]
Northrup Grumman Innovation Systems, Dulles, Virginia, 20166, USA

Brandon Marsell[5]
Kennedy Space Center, Florida, 32815, USA

Russel A. Parks[6]
Marshall Space Flight Center, Huntsville, Alabama, 35824, USA

Propellant tank slosh damping models for launch vehicle ascent analysis typically employ linear models for bare-wall damping, or assume a single, low-amplitude wave height for baffled configurations. A higher fidelity damping model would incorporate nonlinear effects to increase damping as slosh wave amplitude increases. This paper provides an overview of a technical assessment performed by the NASA Engineering and Safety Center (NESC) to evaluate lateral slosh damping as a function of lateral force (or wave) amplitude for multiple tank configurations. The increased fidelity of nonlinear slosh damping models, if leveraged, has the potential to reduce over-conservatism associated with the use of linear slosh damping models. This can provide design flexibility to enhance launch vehicle flight control performance, reduce baffle design requirements and/or increase robustness in targeted areas such as control-structure interaction during ascent.

I. Introduction

Propellant tank slosh damping models are typically linear for bare-wall damping, or assume a single, low-amplitude wave height for baffled configurations. A higher fidelity damping model would incorporate nonlinear

[1] Associate Principal Engineer, NASA Engineering and Safety Center, and AIAA Member.
[2] Computational Fluid Dynamicist, Jacobs Space Exploration Group.
[3] Professor and Academic Vice President, Department of Statistics.
[4] Tech Fellow (Guidance, Navigation and Control), Flight Systems Division (Launch Vehicles Unit).
[5] Environments and Launch Approval Branch Chief, NASA Launch Services Program
[6] Aerospace Engineer, Structural Dynamics Test Branch, Test Laboratory.

effects to increase damping as slosh wave amplitude increases. This paper provides an overview of an assessment performed by the NASA Engineering and Safety Center (NESC) to evaluate lateral slosh damping as a function of lateral force (or wave) amplitude for multiple tank configurations [1]. The increased fidelity of nonlinear slosh damping models, if leveraged, could reduce over-conservatism associated with the use of linear slosh damping models. This can provide design flexibility to enhance launch vehicle flight control performance or increased robustness in targeted areas such as control-structure interaction. The increased damping could also be leveraged to reduce design requirements, resulting in cost avoidance (e.g., design and manufacturing costs) and weight savings (e.g., fewer/smaller baffles).

Launch vehicle dynamics models are required to simulate the movement of lateral fluid sloshing in partially filled propellant tanks. These models typically use a single-degree-of-freedom (DOF) mechanical analogy to capture relevant slosh characteristics for each mode of interest in each tank. The objective of this work is to determine an amplitude-dependent damping profile that can be included in these existing mechanical models. This type of liquid slosh is induced when the tank is subjected to a lateral force due to net body-frame accelerations. An example of this motion for the most common case where the cant angle is zero (i.e., body force is parallel to the tank) is shown in Fig. 1.

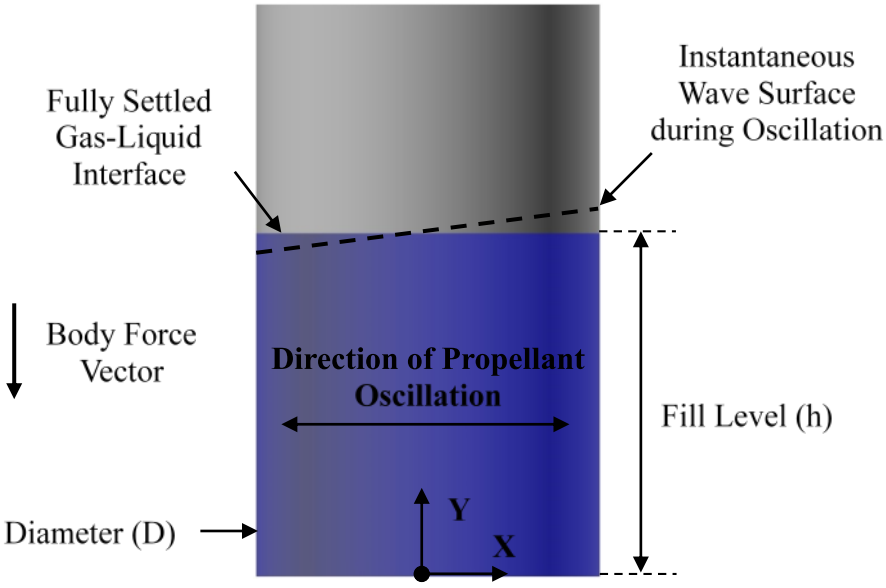

Fig. 1 Illustration of Lateral Liquid Slosh in Cylindrical Tank

Fig. 2 illustrates the most common mechanical analogs for a single slosh mode. The simple pendulum model is defined by the effective pendulum mass, pendulum length, and pivot point location. A rotational damper is added about the pivot point. The spring-mass-damper model is defined by the effective sloshing mass, spring constant, damper value, and location of the force application point [2,3]. Both models break the total fluid volume into a portion that participates in lateral sloshing motion and a portion deeper in the tank that acts as if it is fixed to the vehicle. This fixed mass is not illustrated in the figure. Breakup of the fluid into distinct portions is done to preserve the bulk force and moments on the tank. Model parameters for the sloshing portion of the liquid are calculated first from analysis results or test data of forces and moments on the tank during sloshing. Then, the fixed mass and its location are calculated to preserve the total liquid mass and center of mass location for a quiescent liquid condition.

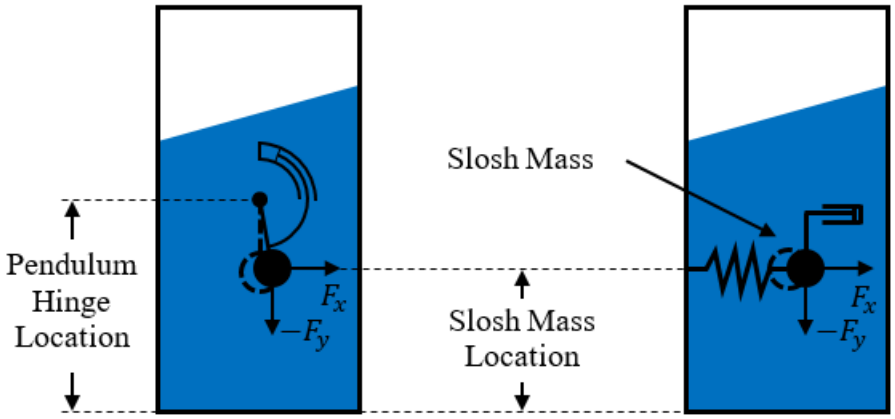

(a) Simple Pendulum Model ***(b) Spring-Mass-Damper Model***

Fig. 2 Illustrations of Simple Mechanical Models of Lateral Liquid Slosh

Both models are well suited to represent relatively small-amplitude waves, where the liquid moves laterally as a bulk mass and the fluid dynamic characteristics do not change with wave amplitude (i.e., linear regime slosh). At larger wave amplitudes, complex fluid motion can develop as energy is transferred from lower to higher order modes. The fluid dynamic parameters at large wave amplitudes depend on the wave amplitude, thus becoming nonlinear. Liquid surface breakup can occur in the nonlinear regime at sufficiently large wave amplitudes. Thus, a sloshing liquid in the nonlinear regime behaves less like a simple harmonic oscillator as the wave amplitude increases. The bulk motion of a slosh wave can be described with these simple models with modification to the pendulum or the spring-mass-damper parameters. This paper concentrates on the spring-mass-damper analogy augmented with a nonlinear damping model that is a function of slosh wave amplitude.

II. Approach

The development of nonlinear damping models was accomplished through a combination of computational fluid dynamics (CFD), testing, and analysis. Emphasis was placed on developing models for cylindrical, SLS Core Stage (CS) liquid oxygen (LOx) and Exploration Upper Stage (EUS) LOx propellant tanks (Fig. 3). Baffled and bare (i.e., unbaffled) subscale tanks were evaluated with distilled water as the fluid. The technical activities completed as part of this assessment included (also summarized in Table 1):

- Evaluation of the scalability of nonlinear slosh damping by performing CFD analysis of high-amplitude slosh dynamics for three sizes of cylindrical tanks (i.e., 43-, 28-, and 18-inch diameter).
- Performance of complementary CFD and testing for the bare EUS LOx tank. The test suite included liquid levels across the height of the tank, with multiple initial wave amplitudes evaluated for each liquid fill level.
- Performance of complementary CFD and testing for the upper dome and cylindrical section of the bare-walled subscale SLS CS LOx tank with a flat bottom. Multiple liquid levels and initial wave amplitudes were evaluated.
- Performance of complementary CFD and testing with multiple liquid levels and initial wave heights for the following baffled configurations:
  - Upper dome and cylindrical section using a flat-bottomed tank with two upper baffles.
  - Cylindrical tank with a domed bottom and a baffle mounted between the flanges of the lower dome and the cylindrical section. Multiple liquid levels were evaluated in the cylindrical section above the dome-barrel interface.
  - Cylindrical tank with a baffle rigidly mounted between two adjoining cylindrical sections.

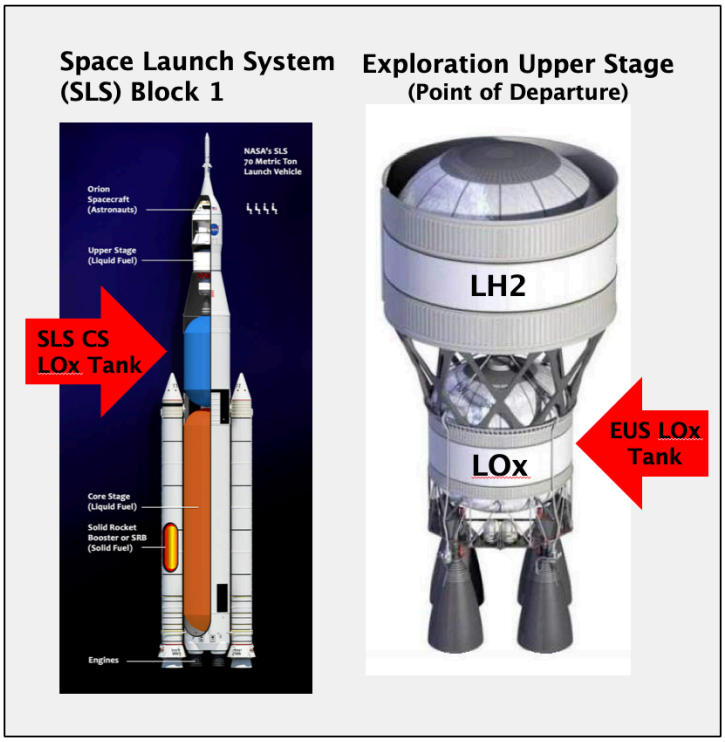

Fig. 3 LOx Tank Locations on SLS Core Stage and EUS

Table 2. Tank Configurations Tested and Analyzed

Tank Configuration	CFD	Testing	GP Models
Cylindrical tanks (three sizes; bare tank)	✓	performed for a single diameter and fill level	performed for a single diameter and fill level
SLS CS LOx tank (bare tank)	✓	✓	✓
EUS tank (1/5 scale) (bare tank)	✓	✓	✓
SLS CS LOx tank (1/7.6 scale) (baffles at dome-barrel interface and in barrel section; fill levels in barrel and upper dome)	✓	✓	✓
SLS CS LOx tank (1/7.6 scale) (single baffle at lower dome-barrel interface; fill levels in barrel section)	✓	✓	✓
Cylindrical tank (single baffle)	✓	✓	✓

For each configuration tested, multiple liquid fill levels were evaluated and numerous tests were conducted for each fill height. First, low-amplitude forcing functions with frequency content across the range of interest were applied at each liquid level tested. The test tank response was used to determine parameters for linear mechanical

propellant slosh models. Second, free-decay tests at multiple initial slosh wave amplitudes were conducted to evaluate damping for a range of wave amplitudes. The same set of test conditions was applied twice for each free-decay run to aid in understanding repeatability and to decrease uncertainty in the test results. Analysis was conducted using multiple methods to extract damping as a function of lateral force amplitude from the free-decay force measurements. The methods were refined throughout the assessment to generate a clean set of damping data points (i.e., minimizing noise and non-lateral sloshing characteristics) and understand the underlying physics behind unanticipated damping data characteristics. The sets of damping data for each fill level were integrated into a single Gaussian Process (GP) model that included the run-to-run uncertainty in the mean line. Use of wave amplitude as an independent variable was evaluated by comparing models that estimate wave amplitude by: (1) analytical conversion of the lateral slosh force to amplitude, and (2) wave amplitude measurements captured by video. Complementary CFD analysis was performed, which aided in the physical interpretation of results and the identification of sensitivities that could skew test data. Furthermore, direct comparison was useful for understanding CFD accuracy and uncertainty for alternate tank configurations where the model may rely on CFD analysis (i.e., absence of test data).

III. CFD

CFD analysis was completed for many of the tested fill levels using Loci-STREAM-VOF. The inclusion of CFD results to testing aided in the physical interpretation of results, and the identification of sensitivities that could skew test data. Furthermore, direct comparison was useful for understanding CFD accuracy for alternate propellant tank configurations where the model relied on CFD analysis results in the absence of test data. This section summarizes the overall approach for conducting CFD analysis and calculating the corresponding slosh damping. This analysis was conducted independently from the evaluation of the corresponding slosh test results, with the exception of developing consistent forcing functions and using consistent data analysis processes. The displacement function captured during testing was used to determine a representative CFD forcing function to mitigate differences between CFD and test results due to initial conditions (see Fig. 4). A representative acceleration profile was used to drive the tank, where large slosh responses were generated by driving the tank near its natural frequency, as determined from low-level initial testing.

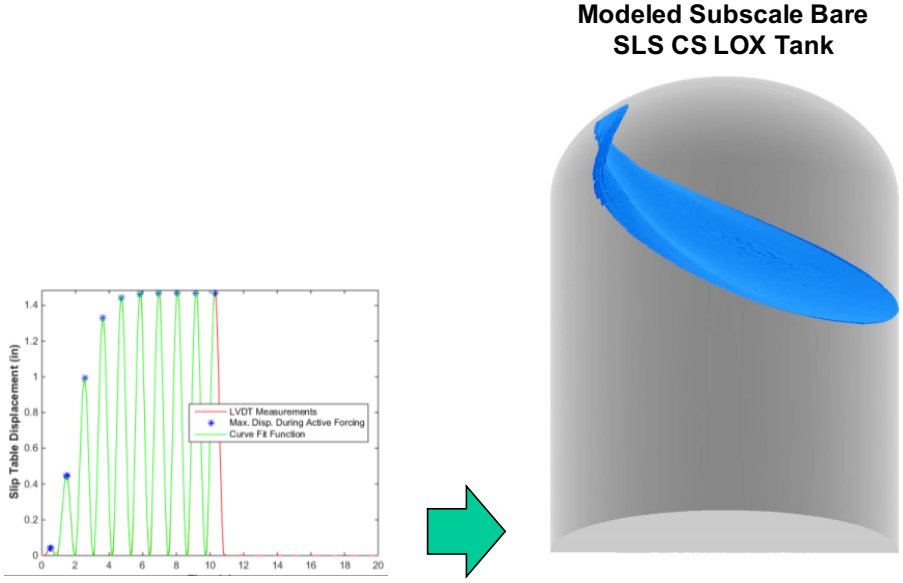

Fig. 4. Sample Forcing Function used for CFD Analysis

A limited range of force amplitudes was assessed for each CFD run. Windows were selected within the range of forces tested to reduce run time, as shown in Fig. 5. The free decay from an initial condition was simulated for multiple conditions. Simulating multiple short periods of free decay was generally more computationally efficient and reduced simulation time versus simulating the entire decay of a single high-amplitude slosh wave. The flow field at various peak slosh wave amplitudes during the tank oscillation was used as the natural slosh wave initial

conditions for free-decay simulations. Fig. 6 illustrates the typical slosh wave amplitude growth observed while forcing the tank at its natural frequency. The slosh wave conditions chosen as initial conditions for free-decay simulations for the example shown are depicted by open circles. The gas-liquid interface shape for each simulation was initialized as a half-period sinusoid in the horizontal plan.

The computational domain consisted of the bare tank interior. A previous computational mesh dependence study [4] was used to guide mesh requirements for the considered cylindrical propellant tanks.

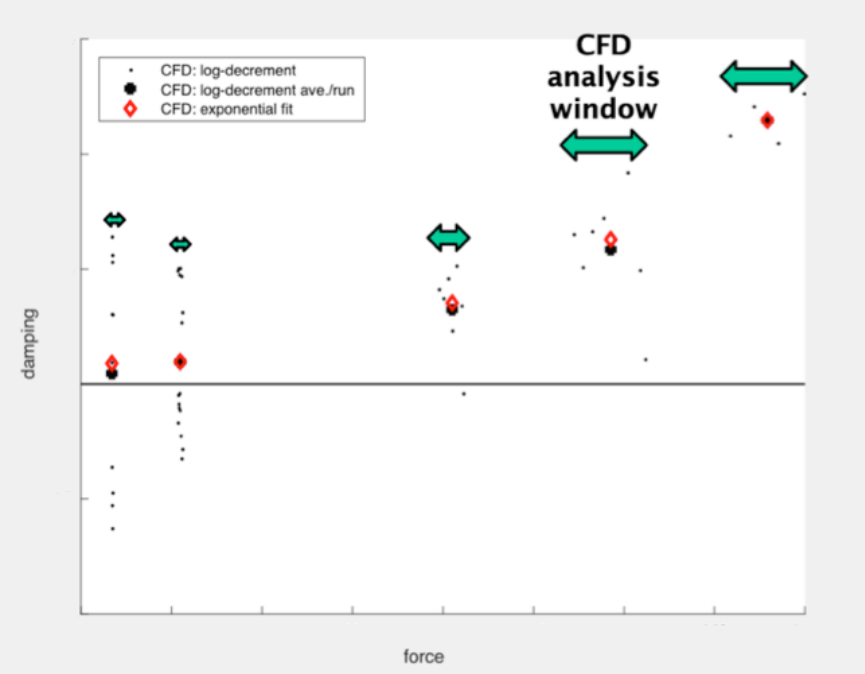

Fig. 5. Sample CFD Results for Bare-wall SLS CS LOx Tank

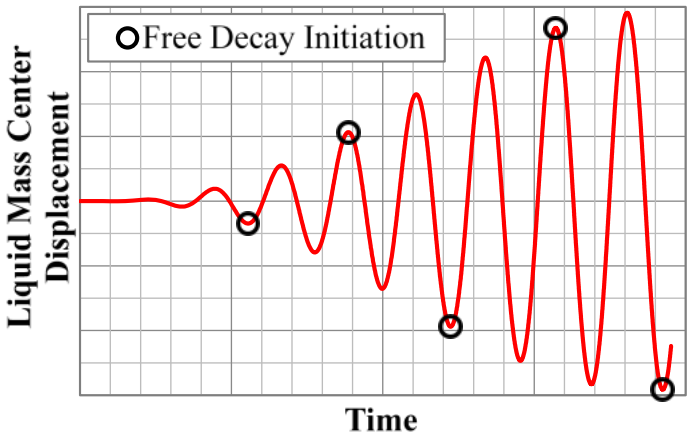

Fig. 6. Example of Natural Slosh Wave Initial Conditions Obtained by Driving the Tank

Slosh damping was calculated from simulation results of freely decaying slosh waves for every half-period of the free-decay CFD simulation results. Slosh mass was calculated to ensure consistency of the proposed slosh model with the predicted lateral slosh force. Specifically, the particular solution to the linear spring-mass model was used

with input from CFD simulation results to calculate the slosh mass. An overview of the methods used to extract damping from CFD analysis is provided in this section. The reader is referred to [1] for details regarding the use of CFD results to calculate the remaining mechanical slosh model parameters.

The slosh damping ratio, ζ, is calculated peak-to-peak based on Eq. (1) where x_i is the total liquid mass center displacement of peak i.

$$\zeta = \ln\left(\frac{|x_i|}{|x_{i+1}|}\right)/\pi \tag{1}$$

An illustration of a typical total liquid mass center displacement history is shown in Fig. 7 with the peak values at times t_i and t_{i+1} used to calculate ζ. Mean damping values were calculated by fitting the x_i values over a chosen sample period to exponential decay curves. This method of calculating mean damping is consistent with the behavior of the simple mechanical models used to represent slosh waves as they decay exponentially. Exponential curve-fit and peak-to-peak methods were used to obtain damping results across each analysis window. The peak-to-peak method is similar to that used to extract the damping from the test results, whereas the exponential curve-fit gives a best-fit result across the analysis window. Both methods are shown in Fig. 8 for an example simulation run.

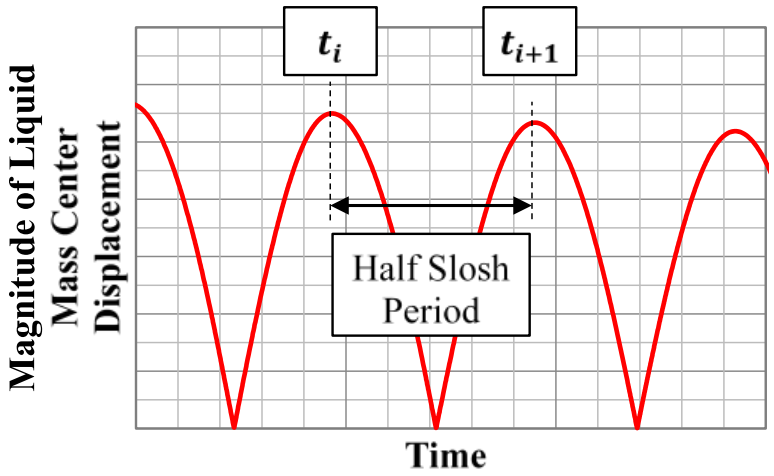

Fig. 7. Typical Total Liquid Mass Center Displacement History for Free-decay Simulations

An example of damping results across a set of simulations at a particular fill level is provided in Fig. 8 for the subscale EUS LOx tank. In this case, the simulation was started six times at different initial wave amplitudes. The damping was calculated using one or more exponential curve fits across the length of the simulation, with each curve fit resulting in a single damping value as a function of wave amplitude. Thus, one or more damping points result from each simulation restart. For a subset of the CFD analyses performed during this assessment, the log-decrement method was used, resulting in a second set of damping data points associated with the same CFD result.

CFD damping results were not integrated into the GP model for damping. Instead, they were plotted with the test-based GP model results for comparison. The CFD analysis provided intuition regarding the fluid dynamics in various scenarios. The results provide context for the use of CFD in the future for full-scale propellant tank testing and when subscale tank test results are not available.

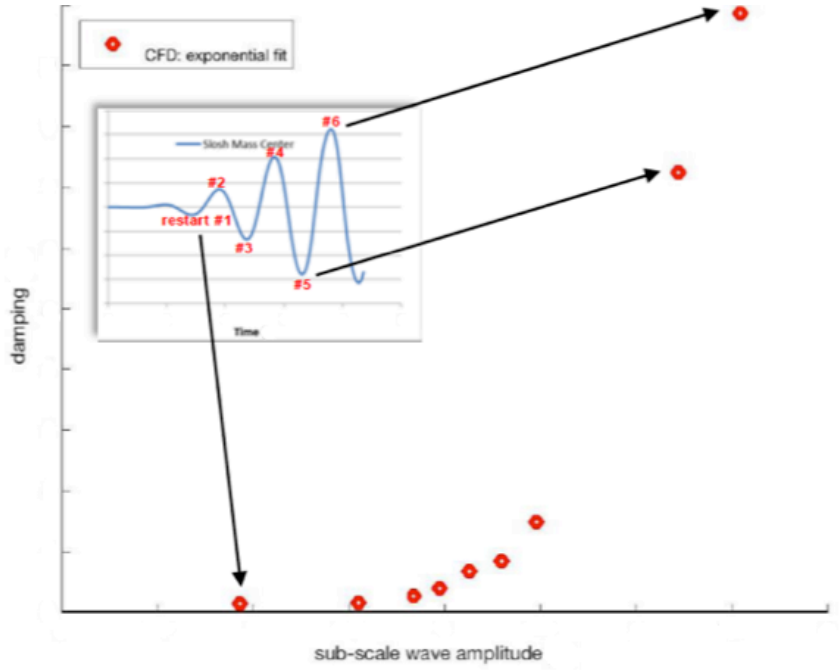

Fig. 8. Sample CFD Slosh Damping Results from Multiple Simulation Restarts

IV. Lateral Slosh Testing

This section discusses the lateral slosh test setup and approach for conducting tests to determine the linear model parameters and nonlinear damping as a function of lateral force (or wave amplitude). The test configuration consisted of a subscale tank of interest in an instrumented test fixture mounted to a slip plate, the top of which could slide freely in one direction while the bottom was grouted to the rigid concrete floor (see Fig. 9). The fixture bolted to the slip table consisted of a base plate, support legs, and a tank support ring, which was designed to be rigid in the bandwidth of interest. The water height within the tank was measured using a measuring tape or a rod with fill height marks. A data acquisition system controlled by a Windows® desktop workstation was used to generate forcing functions and record data.

Force was applied using a hydraulic actuator, which was then used to hold the fixture position constant during free decay of the sloshing wave. This actuator had an internal linear variable displacement transducer (LVDT) to measure armature displacements and a dynamic load cell to measure the dynamic force inputs.

Load cells were embedded and accelerometers were mounted to the test fixture to measure transmitted forces by the sloshing fluid, as shown in Fig. 10. Force and acceleration measurements were conditioned and post-processed to calculate 6-DOF force and moment measurements. The processed force measurements along the horizontal axes (parallel and perpendicular to the direction of the hydraulic actuator force) were combined to become the lateral sloshing force. Note that in the absence of fluid rotation the total lateral sloshing force would be in the same direction as the force from the hydraulic actuator.

High-speed video data were acquired to determine slosh wave heights and capture overall characteristics of the slosh waves for the higher amplitude testing. A flexible measuring tape was adhered to the tank interior surface to facilitate calibration of the wave height video and provide a real-time estimate of wave height during testing.

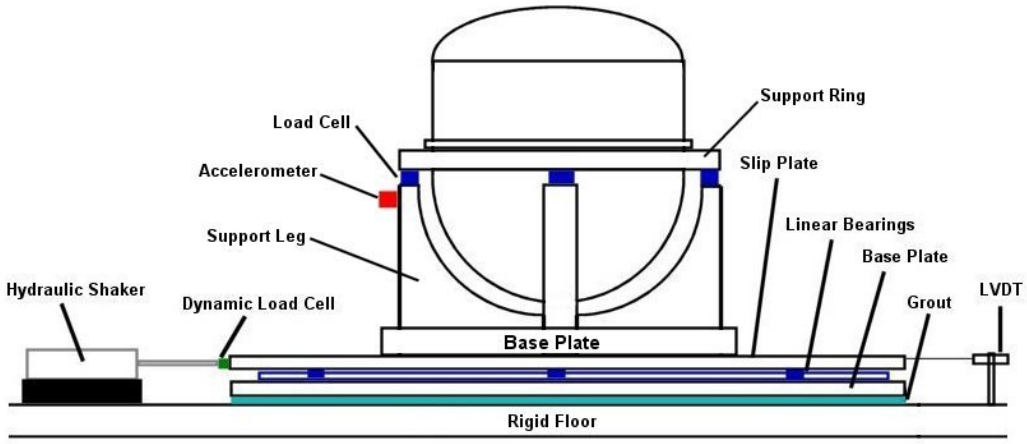

Fig. 9. Lateral Slosh Test Setup

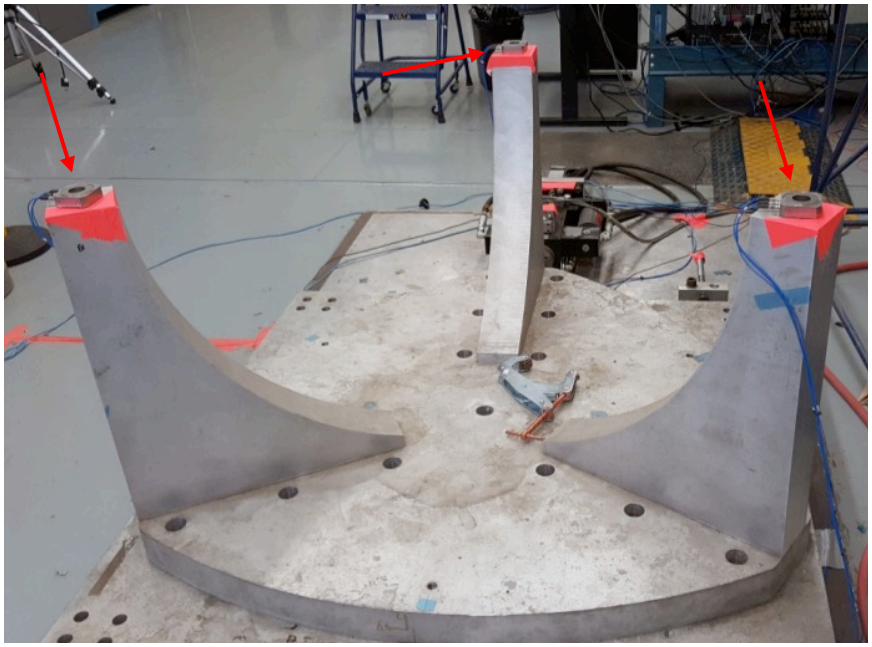

Fig. 10. Force Sensors indicated by Orange Arrows

Slosh tests with low-amplitude random force excitation were conducted to determine slosh mass, frequency, and damping. Frequency content was restricted to between 0.5 and 5 Hz to avoid exciting higher order fluid modes. The forces were filtered, and real-time frequency response functions (FRFs) were calculated over the same bandwidth for data quality evaluations. The results were post-processed to estimate slosh parameters for the first asymmetric slosh. The full set of linear slosh parameters for each configuration, liquid level, and method are provided in Appendix A of [1]. Those used for analytical conversion from force to amplitude are summarized in Appendices E1 through E4.

A majority of the tests were performed to determine damping as a function of force, which can be converted to wave amplitude. The excitation method for these tests was to apply a sinusoidal input to the test fixture at or near the frequency of the slosh mode of interest, typically using a forcing function with a smooth, gradually increasing amplitude. The tank was quick-stopped at a point close to zero velocity in effort to minimize transients, and the residual horizontal forces were recorded as the slosh wave decays. The time histories were post-processed to

determine the slosh parameters of interest. The wave heights, in some cases, were viewed with a real-time high-frame-rate video feed using a camera aimed at a measuring tape adhered to the tank interior surface. The hydraulic actuator was used to apply the excitation and to hold the fixture rigid.

During the free decay of the slosh wave, there was sometimes a slow change in the slosh direction. This phenomenon is discussed in [2], Section 3.4, and occurred most frequently with large input excitations at the fundamental slosh mode frequency. It is believed that a tank eccentricity, or out-of-roundness, exacerbated this effect. The subscale SLS CS LOx tank was observed to have as much as a 0.625-inch difference in diameter between axes. Further, the out-of-roundness of the subscale tanks resulted in two slosh modes close in frequency, roughly 90 degrees in orientation from one another. Slosh rotation can result in a transfer of energy from one mode to the other. One concern with the introduction of fluid rotation during the free-decay tests was its effects on the lateral damping estimates, since damping was calculated from the free decay in the axis of excitation. When the fluid is rotating, the kinetic energy effectively decreases from the excitation axis as the slosh wave rotates off this axis. For this reason, the damping values estimated would appear higher than if damping were estimated in the same configuration without rotation. Another concern was the complexity introduced to the damping analysis. Efforts were made to orient the tanks such that the driving force was along the semi-major axis, which decreased the slosh wave's propensity to rotate. However, this was a time-consuming process that was exacerbated by the changing location of the semi-major axis along the tank height. Therefore, slosh rotation was present in much of the collected data.

While fluid rotation was an undesirable feature for isolating and quantifying lateral sloshing dynamics, it may be present in full-scale systems. Evaluation of ovality and discontinuities from manufacturing of full-scale tanks and their effect on slosh rotation would be relevant for the launch vehicle propellant slosh dynamics. However, this was outside the scope of this assessment.

V. Data Analysis

The analysis approach for this section was used consistently across all free-decay data sets to establish a damping model for each tank configuration and fill height. This approach evolved as idiosyncrasies of various tests challenged the analysts to refine the approach. After the final process was selected, the data from all free-decay tests were rerun using the method outlined in this section.

A. Damping Estimation from Free-decay Force Data

The analysis conducted to estimate damping based on free-decay slosh test force measurement data is summarized in Fig. 11. Prior to evaluating the damping, raw free-decay data were processed by removing the forced response components, eliminating bias, and filtering to remove content above the fundamental slosh frequency. Damping was calculated using the log decrement of the root-sum-square (RSS) for each of the free-decay tests (i.e., all subscale tank configurations, liquid levels, and initial wave amplitudes) conducted during this assessment. In scenarios where the lateral sloshing motion was obscured by fluid rotation during the test, damping results were improved by optimizing the slosh damping and other parameters (i.e., slosh wave amplitude, natural frequency, phase angles, and data biases) to best fit the basis functions to the slosh data across a specified window. This method was useful for improving damping estimates and understanding the relationship between test data peculiarities and slosh rotation.

Damping results were calculated for each free-decay test as a function of the lateral sloshing force magnitude. For reference, these results were converted to damping as a function of estimated slosh wave amplitude. This conversion provided context regarding the size of sloshing waves associated with a given amount of damping.

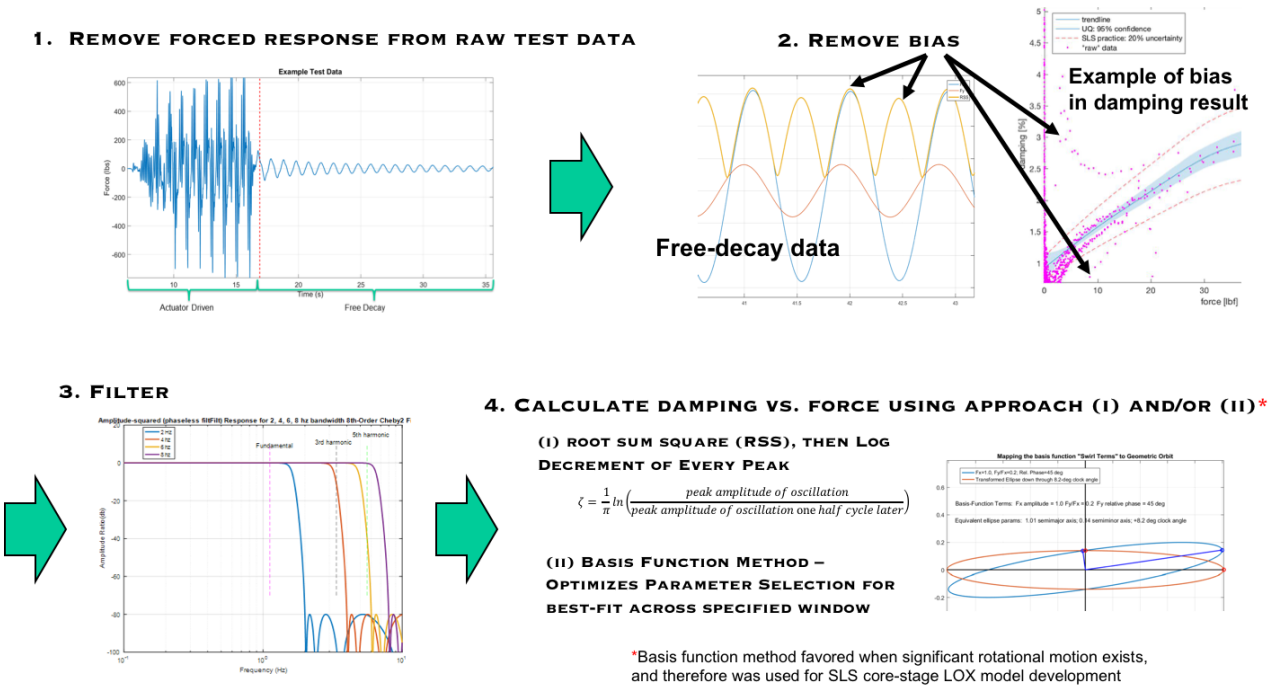

Fig. 11. Process for Calculating Damping versus Force from Free-decay Data

B. Wave Amplitude Estimation from Force Measurements

The acquired force measurements can be used to estimate slosh wave amplitude using linear theory (i.e., a second-order model) combined with estimates for slosh mass, slosh frequency, and a geometry-specific conversion factor. The analytical conversion is described in Appendix B1. For this assessment, slosh mass and slosh frequency estimates were produced by testing and CFD analysis. The estimates determined from random vibration testing were used for the conversion of the independent variable in the test-based damping models from force to wave amplitude. The conversion factor, Γ, was estimated using the Southwest Research Institute (SwRI) SLOSH code for a given geometry and liquid level and relates the slosh mass displacement, x_S, to the slosh wave amplitude, η [3]. The SLOSH code is based on the long-standing theory described by Lomen [5], which has been used by multiple organizations to calculate non-damping slosh model parameters for launch vehicles. Γ is calculated using what is essentially a potential flow solution of a small amplitude slosh wave and is a function of tank geometry and liquid level.

C. Wave Amplitude Estimation from Video Data

An alternate method of estimating wave amplitude (and slosh damping versus wave amplitude from these measurements) used processed video data. This is a more direct method compared with analytical conversion of force data for determining damping models as a function of wave amplitude.

A tool was developed to automate the extraction of wave amplitude from video data but tracking the wave motion around baffles often required user interaction to make a best estimate of the slosh wave amplitude due to obscured waves, lighting artifacts, and/or challenging surface characteristics. Efforts were made during the test setup to provide high-quality video through the selection of background and lighting, as shown in Fig. 12. This improved the automated video-processing capability, but the surface characteristics created challenges that required significant user involvement during processing for high-amplitude tests with baffles. For low-amplitude waves, as shown in Fig. 13, it is relatively straightforward to track the surface-tank interface. However, as the wave amplitude increases, it becomes more difficult to estimate the free surface location. This difficulty can be observed from the still frames shown in Fig. 14. In this scenario, where the detected edge may be several pixels in height, the centroid of the detected blob was used as the observed wave height for the frame.

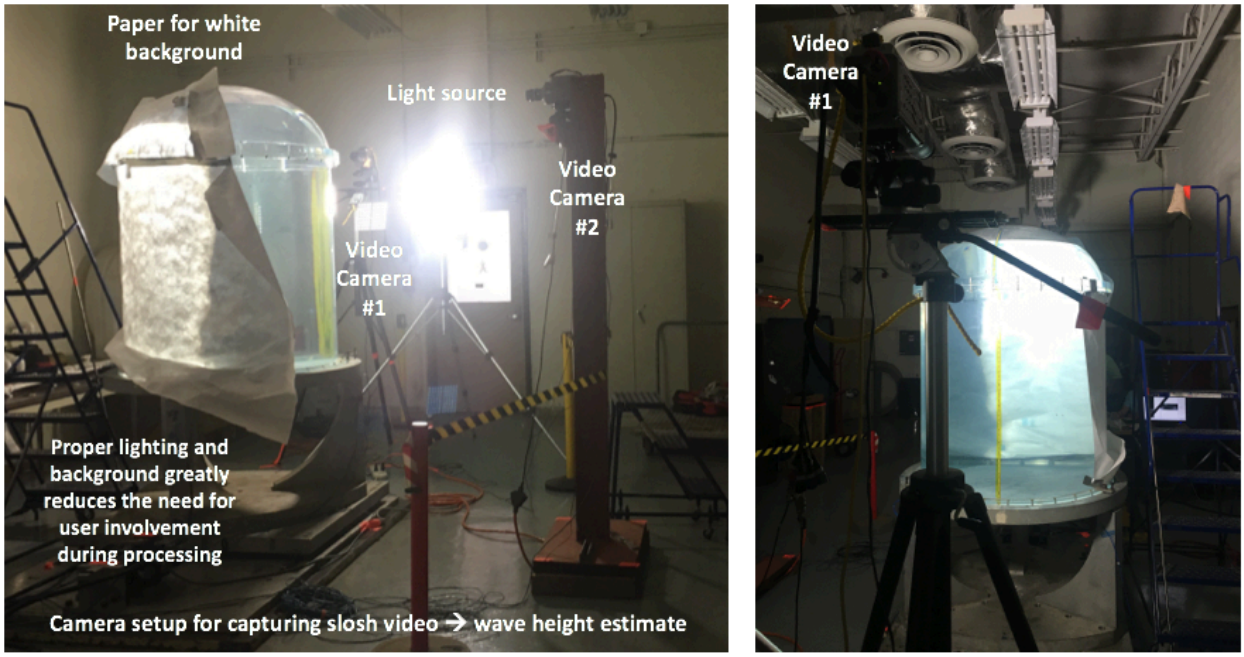

Fig. 12. Video Camera Setup for Slosh Testing

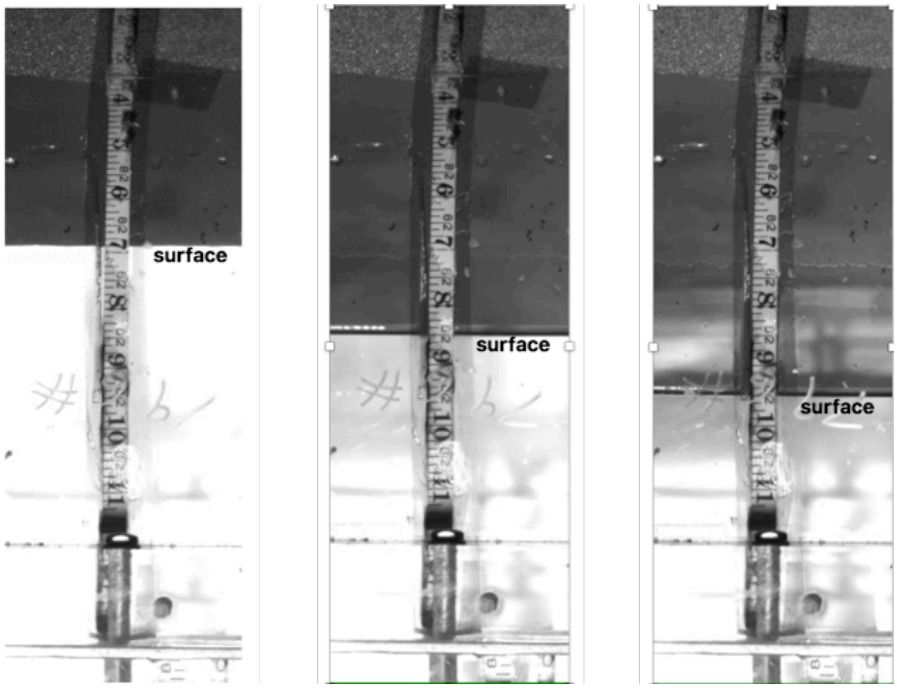

Fig. 13. Still Frames from Video of Low-amplitude Wave (surface-tank interface indicated)

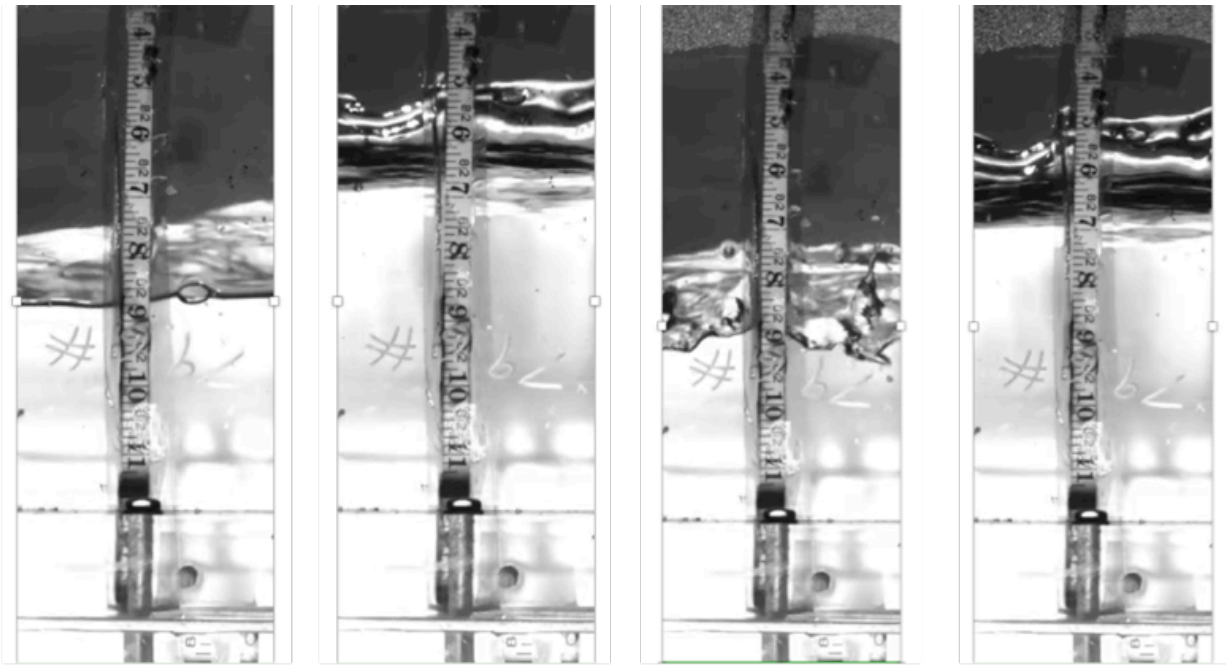

Fig. 14. Still Frames from Video Recording of High-amplitude Wave

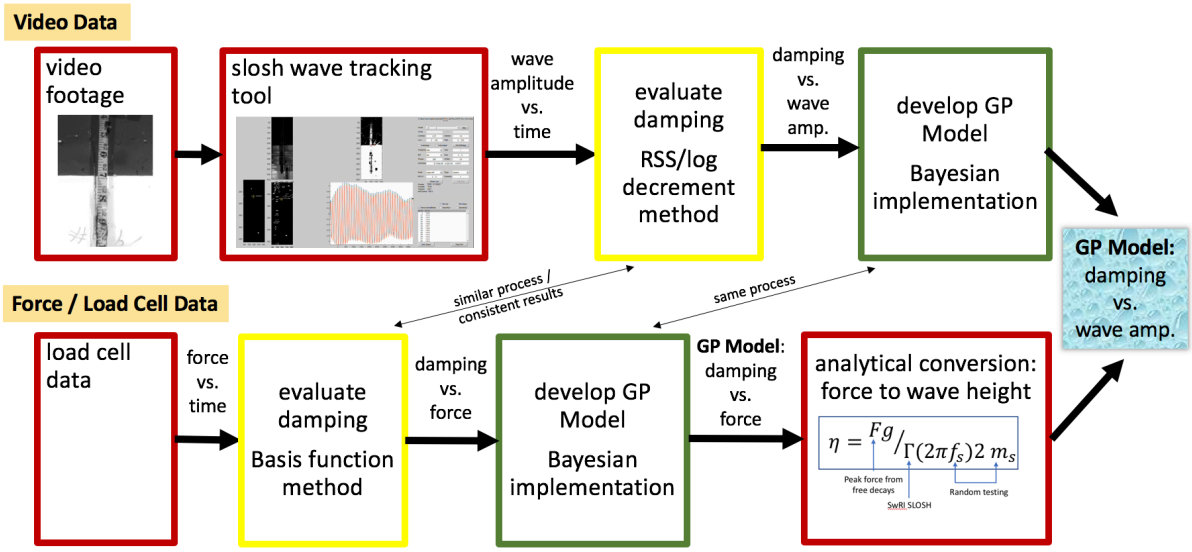

Fig. 15. Comparison of Processes for Analyzing Video and Load Cell Data

Video data were processed for only a subset of the slosh tests. The data were used to provide a second set of damping curves as a function of wave amplitude. These curves were compared to the damping versus wave height results, found indirectly using Γ and the slosh mass/frequency from the random vibration tests. In summary, two methods were used to estimate the wave amplitude from the indicated test data:

1. Analytical conversion of force measurements to wave amplitude.
2. Estimation from video data.

A block diagram comparing the two processes for determining the GP model of damping as a function of wave amplitude is shown in Fig. 15.

D. Development of GP Models with UQ

The evaluation of damping based on measured force (or wave amplitude) from free-decay testing discussed in the previous sections results in a set of discrete damping points as a function of force/wave amplitude for each free-decay test. This section describes the approach taken to use these data to estimate the mean damping curve and quantify the run-to-run uncertainty associated with that estimation.

Among the vast number of possibilities for a single, unified statistical model to accommodate estimation of the linear and nonlinear damping regions, a Bayesian implementation of a GP formulation was selected for the following reasons:

- GP models do not have discontinuities (i.e., they are infinitely differentiable (smooth)).
  - The Bayesian approach relies on a pre-established "prior" set of smooth functions (see Fig. 16, where each curve represents a random sample from GP prior distribution).
- GP models do not assume a specific parametric form, as with a curve fit, and can accommodate a wide variety of curve shapes (i.e., flexible).
- The Bayesian approach is extensible and can accommodate multiple data types and uncertainties.
  - Capable of combining experimental and computational models.
  - Accommodates uncertainties from multiples sources.

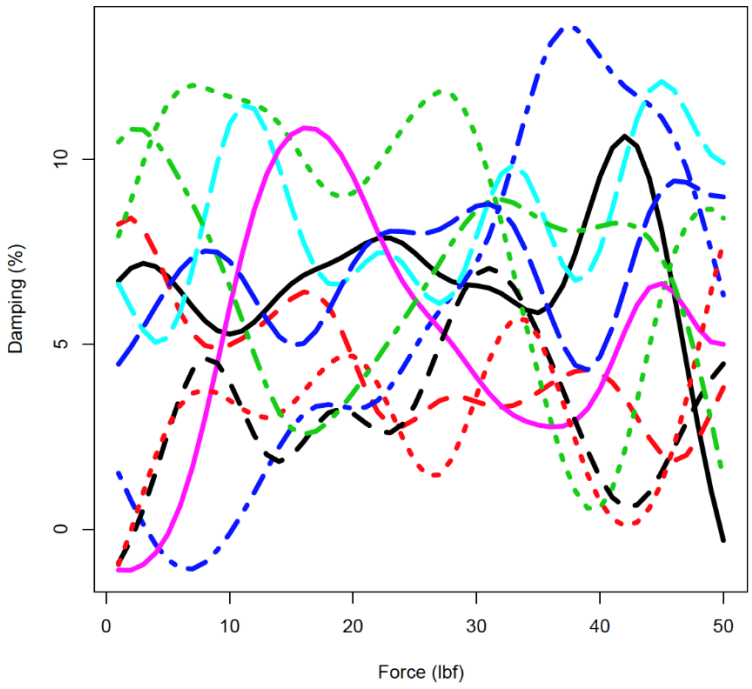

Fig. 16. Example Set of GP Prior Realizations

GP models were developed for the experimental results only. Interim GP models with uncertainty quantification (UQ) were developed that incorporated CFD and test results into a single integrated model, but the final model deliveries for each subscale tank configuration isolated the test results for clarity. Inclusion of the CFD results would have the benefit of decreasing the uncertainty in the mean line and providing a framework for quantifying the discrepancy between the CFD and the GP model.

GP models were developed using all subscale tank test runs at a given fill height. An interim step was to produce a GP model for each set of runs at a given initial wave amplitude and fill height. A derivative test was incorporated for each set of runs at a given initial wave height to exclude data at high force values (i.e., beginning of free decay) where the damping curve becomes non-monotone. These sets of GP models were combined to form a single model per fill height (see Fig. 17).

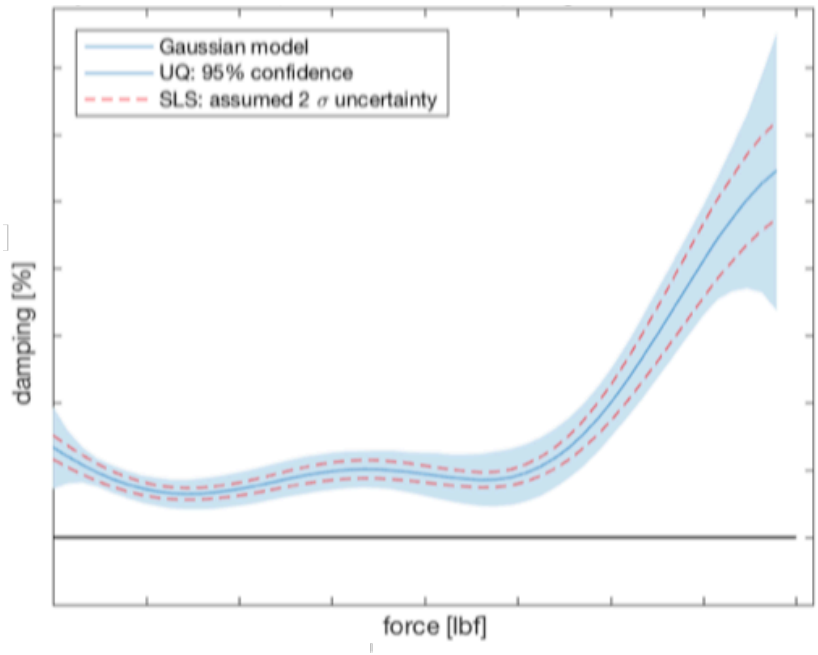

Fig. 17. Example of Combined GP Model and UQ, All Initial Conditions

Several idiosyncrasies related to the slosh data were managed as part of the GP model development, including:

- The model smoothness prior distribution "knob" was adjusted manually to capture features without excessive wiggles. The intent was to capture trends and key features but not every wiggle in the test data.
- At low-force levels, data were excluded from the model since the statistical analysis revealed that extrapolating the damping model to zero force produced lower uncertainty in this region as compared with using all the test data.
- Negative damping values were excluded from the GP model. A negative damping value for a given mode implied energy was transferred from another mode or slosh rotation. This provided a better fit overall without spurious negative damping values. For models at some fill levels, this contributed to a negative damping slope at low force. However, the data analysis process was maintained across all models for consistency.
- When multiple "families" of data were present, the GP model was based on the more conservative (i.e., lower damping) of these families.

For this effort, the final product for each configuration and fill height was a single fitted GP model for the damping curve as a function of force and associated uncertainties. Often, the development of the GP models took several iterations between the statisticians and engineers to determine how to refine the analysis process, manage model discrepancies, and agree on an appropriate level of smoothness for the curve fit.

VI. Sample Results

Results from testing include linear slosh model parameters, damping data points, and nonlinear GP models of damping as a function of lateral force (and wave amplitude for reference). The test-based results were augmented with slosh model parameters and damping data points evaluated independently based on CFD. A sample data set for a single liquid fill level in a bare wall tank is provided in Fig. 18, and sample trends for a different bare wall tank are

provided in Fig. 19. Data were produced for bare cylindrical tanks, a bare subscale SLS CS LOx tank (upper dome and barrel section), a bare subscale EUS LOx tank, a baffled cylindrical tank, and baffled subscale SLS CS LOx tanks. Comparisons were made between test, CFD, and existing models for bare wall [2,3] and baffled configurations [6].

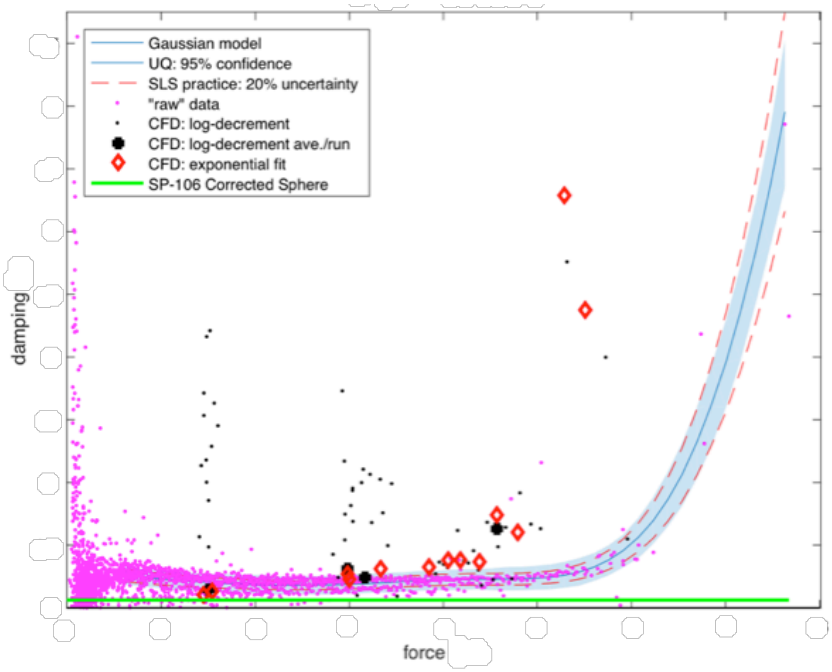

Fig. 18. Example Nonlinear Damping Data Set

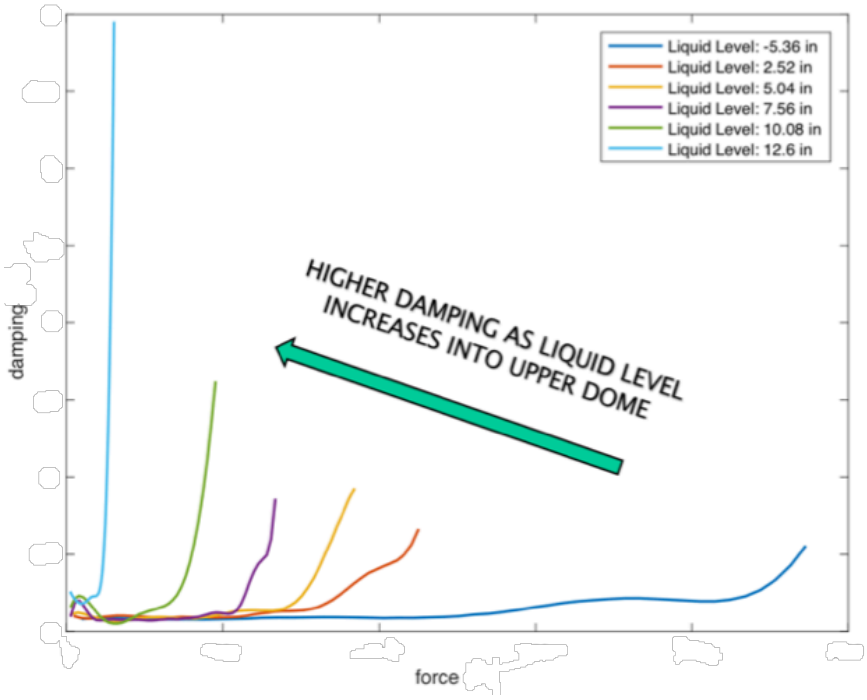

Fig. 19 Nonlinear Damping Model Trends (Mean Lines from Multiple Fill Levels)

VII. Conclusions

This paper provided an overview of the testing and analysis conducted as part of a technical assessment performed by the NASA Engineering and Safety Center (NESC) to evaluate lateral slosh damping as a function of lateral force (or wave) amplitude for multiple tank configurations. In particular, slosh testing, CFD, and data analysis was conducted in order to increase fidelity in slosh models for launch vehicle liquid propellant tanks where merited. The paper discussed the tank configurations considered, lateral slosh test setup, data analysis processes employed for the development of slosh damping models, CFD analysis approach, and sample nonlinear damping results. Damping models developed following these processes were leveraged for SLS flight controls design following the processes outlined in [7,8]

VIII. Acknowledgements

The authors gratefully acknowledge the contributions from additional team members for supporting this effort. This includes Ravi Purandare and Joseph Powers for slosh modeling expertise; Daniel Lazor for modal and video analysis; Hong Yang for CFD analysis; Alexander McCool, Dana Chandler and Marlon Holt for slosh testing; and Jeffrey Brouwer for uncertainty analysis. The authors are thankful for NESC support from Loutricia (Tricia) Johnson (program analyst), Jonay Campbell (technical editor), Melissa Strickland (project coordinator), and Linda Burgess (scheduler). The authors also wish to thank consultants Robert Hall and John Ottander (launch vehicle flight controls); Chad Eberhart (video setup and data analysis); Cornelius (Neil) Dennehy (NESC Guidance Navigation and Control Technical Fellow); and David Schuster (NESC Aerosciences Technical Fellow).

References

[1] VanZwieten, T.S., Brodnick, J. M., Brouwer, J. R. Ruth, M., Marsell, B., Purandare, R. Y., Powers, J. F., Parks, R. A., Holt, M. R., "Nonlinear Slosh Damping Analysis for Launch Vehicle Propellant Tanks," NASA TM-2019-220278, 2019.

[2] Abramson, H., Norman, B., Helmut, F., et al., "Dynamic Behavior of Liquids in Moving Containers," NASA SP-106, National Aeronautics and Space Administration, 1966.

[3] Dodge, F. T., "The New 'Dynamic Behavior of Liquids in Moving Containers,'" Southwest Research Institute, 2000.

[4] Yang, H. Q. and West, J. S., "Non-Linear Slosh Damping Model Development and Validation," 62nd JANNAF Propulsion Meeting, June 2015.

[5] Lomen, D. O., "Liquid Propellant Sloshing in Mobile Tanks of Arbitrary Shape," NASA CR-222, 1965.

[6] West, J., Westra, D., Yang, H. Q., Brodnick, J., and Sansone, M., "Extension of Miles Equation for Ring Baffle Damping Predictions to Small Sloshing Amplitudes and Large Baffle Widths," JANNAF, Abstract Number: 2016-0006BW, December 2016.

[7] Ottander, J. A., Hall, R. A., Powers, J. F., "Practical Methodology for the Inclusion of Nonlinear Slosh Damping in the Stability Analysis of Liquid-propelled Space Vehicles", AIAA SciTech, AIAA 2018-2097, 2018.

[8] Hall, R., Bertaska, I., and Powers, J., "Space Launch System Implementation of Nonlinear Slosh Damping Models for Flight Control System Design," JANNAF, December 2019.